Solar Energy Materials & Solar Cells 288 (2025) 113650

Contents lists available at ScienceDirect

Solar Energy Materials and Solar Cells

journal homepage: www.elsevier.com/locate/solmat

Is TOPCon ready for EVA? Insights from damp heat testing of glass-backsheet modules

Xinyuan Wu [a,*], Wei Wu [b], Yan Zhang [b], Jiexi Fu [a], Xutao Wang [a], Jieyi Li [a], Weiguang Yang [b], Feng Li [b], Lin Lv [b,**], Jessica Yajie Jiang [a], Bram Hoex [a,***]

[a] School of Photovoltaic and Renewable Energy Engineering, University of New South Wales, Sydney, 2052, Australia
[b] Jolywood (Taizhou) Solar Technology Co., Ltd., Taizhou, Jiangsu, 225500, China

ARTICLE INFO

Keywords:
TOPCon
Solar module
Reliability
Damp-heat
Degradation
Ethylene vinyl acetate
Laser-assisted firing
Glass backsheet
Metallization

ABSTRACT

Tunnel oxide passivated contact (TOPCon) technology currently dominates the photovoltaic market, and the industry is now focused on enhancing their cost-effectiveness while ensuring their durability in harsher environments. TOPCon modules commonly use a glass–glass bill of materials that incorporates polyolefin elastomer and co-extruded polyethylene encapsulants. Though, for cost and weight reduction, the use of polymer backsheets and lower-cost encapsulants is appealing. This study investigates the performance of glass-backsheet (G-B) TOPCon modules fabricated with two types of silver/aluminum (Ag/Al) pastes: conventional firing with standard Ag/Al paste and low-Al-content Ag paste combined with laser-assisted firing (LAF). The modules, encapsulated with ethylene vinyl acetate (EVA), were subjected to damp-heat testing. Our findings indicate that solar cells with Ag/Al paste exhibit lower stability compared to low Al-content Ag paste; however, acid-rich moisture conditions contribute to glass-frit failures in both types of pastes. Additionally, the rear-side metal contacts, particularly those containing tellurium (Te) compounds, are susceptible to degradation in such environments. Based on these degradation mechanisms, we conclude that further investigation is required to allow for the wider adoption of EVA in TOPCon modules, particularly when a polymer backsheet is used. Ongoing research is essential to optimize these materials and enhance the cost-effectiveness and reliability of TOPCon technology for future applications.

1. Introduction

Over the past decade, tunnel oxide passivated contact (TOPCon) solar cells have steadily gained global photovoltaic (PV) market dominance, and they are predicted to the dominant technology in the next 5 years [1]. The industrialization of TOPCon technology has driven the development and refinement of its fabrication processes, including precise tunnel oxide layer formation, advanced metallization techniques, and optimized passivation strategies [2–12]. These process advancements have not only enhanced power conversion efficiency (PCE) but also improved the overall durability and operational stability of TOPCon modules, making them well-suited for deployment in diverse climatic conditions. Trina solar recently achieved a world-record PCE of 26.58 % for bifacial industrial TOPCon solar cells, representing a significant milestone in the evolution of high-efficiency PV technologies [13]. This record-breaking achievement underscores the success of continuous process optimization and innovative material integration in pushing the efficiency limits of commercial solar cells.

Despite the rapid progress, TOPCon modules still face stability issues under certain testing and operational conditions, particularly under damp-heat stress. Studies by Sen et al., Zhou et al., and Ye et al. highlighted the potential for degradation in TOPCon modules during long-term damp-heat testing [14–16]. Our previous research suggests that silver/aluminum (Ag/Al) paste may contribute to this instability through redox reactions [17]. Recently, laser-assisted firing (LAF) techniques, such as laser-enhanced contact optimization (LECO), have emerged as effective approaches for reducing or eliminating Al compounds in front-side paste [3,18–24]. These techniques facilitate the activation of ohmic contact formation without relying on Al spikes [25–27]. Notably, the adoption of low Al-content Ag paste enabled by

* Corresponding author.
** Corresponding author.
*** Corresponding author.
E-mail addresses: xinyuan.wu@unsw.edu.au (X. Wu), lvl01@jolywood.cn (L. Lv), b.hoex@unsw.edu.au (B. Hoex).

https://doi.org/10.1016/j.solmat.2025.113650
Received 20 January 2025; Received in revised form 12 April 2025; Accepted 12 April 2025
Available online 21 April 2025

LAF has substantially enhanced the stability of TOPCon solar cells, exhibiting minimal damp-heat degradation in glass-backsheet (G-B) modules encapsulated with polyolefin elastomer (POE) and co-extruded polyolefin, such as the EVA-POE-EVA (EPE) triple-layer encapsulant [18]. This further demonstrates the potential to reduce the levelized cost of electricity (LCOE) for TOPCon modules.

Ethylene vinyl acetate (EVA) has long been the preferred encapsulant for solar modules due to its excellent adhesion to silicon solar cells, high transparency, good processability, and cost-effectiveness, contributing to lower fabrication costs in TOPCon modules. However, EVA has some drawbacks that can impact the long-term performance of PV modules, particularly its tendency to generate acetic acid (CH_3COOH) over time [28–31]. Spinella et al. reported that in passivated emitter and rear cell (PERC) modules encapsulated with EVA, both glass-glass (G-G) and G-B configurations exhibit similar failure mechanisms. However, G-G packaging more effectively mitigates detrimental reactions by reducing moisture ingress, highlighting the protective advantage of a double-glass structure [32]. Sen et al. further demonstrated that EVA G-B TOPCon modules experience a more pronounced relative power loss compared to PERC-based modules, suggesting a stronger sensitivity of TOPCon cells to EVA-induced degradation [14]. Additionally, Iqbal et al. investigated the impact of acetic acid on TOPCon cells using acetic acid solutions, but their approach does not fully replicate real-world module degradation pathways, particularly under prolonged damp-heat conditions [33]. While previous studies have explored failure mechanisms in EVA-based G-G and G-B modules, a significant knowledge gap remains regarding the degradation of metallization under the harsher conditions induced by the hydrolytic degradation of EVA, particularly across different TOPCon technologies. As we previously mentioned, low Al-content Ag paste has been shown to enhance the stability of G-B modules with POE and EPE encapsulants. However, its effectiveness under the more aggressive conditions associated with the hydrolytic degradation EVA has not been systematically studied. Addressing this gap, our study aims to directly investigate the degradation mechanisms of EVA-encapsulated G-B TOPCon modules through module-level analysis following damp-heat testing, providing critical insights into their long-term reliability and failure pathways.

In this study, we evaluated two types of industrial EVA-encapsulated TOPCon modules with different front-side metallization compounds under damp-heat conditions. We identified degradation signatures through module-level characterization. To investigate contact degradation on both the front and rear sides, cell-level samples were delaminated from the modules. Comparisons were conducted between fresh and degraded samples, focusing on variations in the contacts. Additionally, acid mist-treated samples were analyzed to trace potential correlations with EVA-encapsulated modules. We propose potential module-level degradation mechanisms for the front and rear contacts of two mainstream TOPCon solar cells, offering new insights into the reliability of TOPCon solar modules.

2. Experimental details

Two types of solar cells were used in the fabrication of G-B modules for these experiments. All TOPCon cells were manufactured using G10 n-type Czochralski (Cz) silicon wafers with dimensions of 182 mm × 183.75 mm. The key distinction between the two cell types lay in their front-contact metallization. Baseline cells used a standard commercial Ag/Al paste (Al content: 3–5 at.%) applied through a conventional firing process, whereas the other group employed a customized low-Al-content Ag paste (Al < 0.2 at.%) for front-contact formation, combined with a laser-assisted firing (LAF) process under reverse bias conditions. Prior to soldering, all solar cells were half-cut, resulting in modules containing 144 half-cut cells each. Fig. 1(b) illustrates the G-B module schematic, where EVA served as the encapsulant for both the front and rear sides, ensuring robust encapsulation. UV-blocking EVA was applied to the front side, while UV-transparent EVA was used on the rear side of the TOPCon modules. The backsheet was transparent with a white grid design.

The experimental flow, shown in Fig. 1(c), included I-V measurements and electroluminescence (EL) imaging of all modules. Module-level DH85 testing adhered to the IEC TS 62782:2016 standard, with output measurements conducted using a GIV-200DS2616 flash tester from Gsolar Power [34]. After the DH85 testing, I-V parameters and EL images were reassessed to identify degradation fingerprints by Gsolar Power GIV-200DS2616.

After conducting module-level measurements, small module tokens were prepared using an angle grinder or a cordless hollow drill. Both tools are manufactured by Jiangsu Dongcheng Tool Co., Ltd., with the angle grinder model being S1M-FF-100B and the cordless hollow drill model being MJZ1601. These tokens were subsequently heated to delaminate the glass, backsheet, and EVA layers, allowing for the collection of cell tokens for further characterization. Cross-sectional imaging of metal contacts was conducted using a Zeiss 550 Crossbeam cryo-focused ion-beam scanning electron microscope (cryo-FIB-SEM).

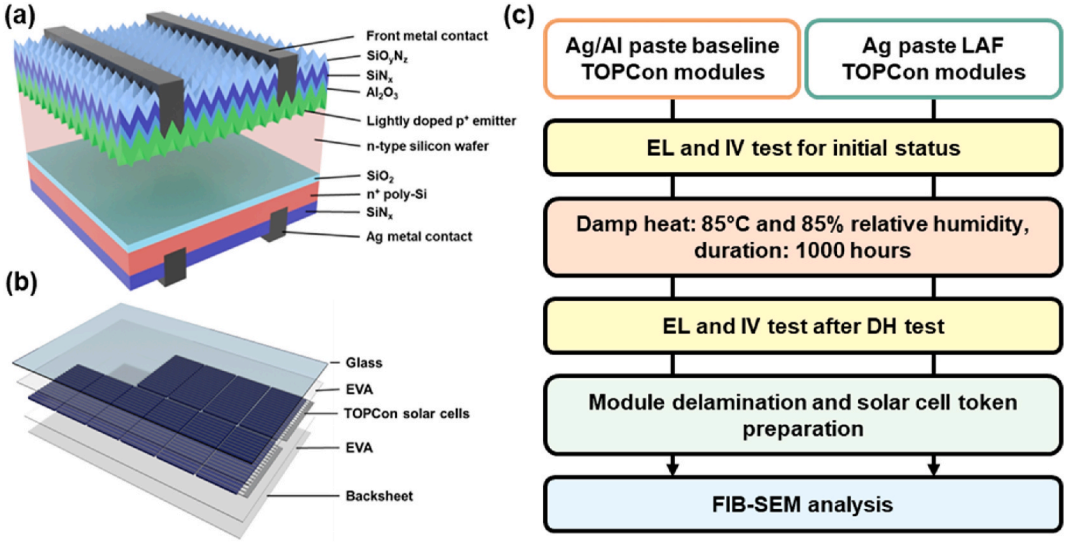

Fig. 1. (a) Schematic representation of the TOPCon solar cells, (b) glass-backsheet (G–B) TOPCon modules utilized in this study, and (c) experimental workflow for module accelerated damp-heat testing.

The SEM operated at a probe current of 7 nA and an electron high-tension (EHT) voltage of 15 kV. During FIB sessions, the stage was tilted to 54° relative to the FIB gun and 36° relative to the sample surface for imaging. The SEM images and scales were adjusted accordingly. For elemental analysis, the FIB probe operated at 30 kV and 50 pA in standard mode. Energy-dispersive spectroscopy (EDS) analysis was performed under identical SEM conditions using the Oxford Instruments Ultim® Max detector. Data processing with the AZtec software provided detailed insights into elemental ratios and distribution [35].

3. Results and discussion

3.1. Module damp-heat testing

Fig. 2 presents a performance comparison of baseline and LAF modules before and after 1000 h of DH85 testing, evaluating key parameters: maximum power output (P_{max}), short-circuit current (I_{sc}), open-circuit voltage (V_{oc}), and fill factor (FF). The baseline modules suffered a substantial 37.0 % relative decline in P_{max}, decreasing from 581.9 W to 366.4 W, whereas the LAF modules demonstrated a much smaller relative reduction of 6.2 %, with P_{max} dropping from 581.1 W to 544.8 W. With respect to the I_{sc}, the baseline modules exhibited a relative decrease of 2.9 % (from 13.7 A to 13.3 A), compared to a 1.5 % reduction in LAF modules (from 13.6 A to 13.4 A).

V_{oc} changes were minimal: the baseline modules showed a 0.2 % decrease (from 53.2 V to 53.1 V), while the LAF modules experienced a slight improvement of 0.2 % (from 51.8 V to 51.9 V). However, the most significant degradation occurred in FF. The baseline modules experienced a dramatic 34.9 % relative reduction in FF, from 79.6 % to 51.8 %, compared to a modest 5.2 % reduction in LAF modules, declining from 82.6 % to 78.3 %.

The primary factor driving output loss during DH85 testing was the significant reduction in FF, with negligible changes in I_{sc} and V_{oc}. Baseline modules showed greater overall degradation compared to LAF modules, aligning with previous findings [18]. Additionally, the use of EVA as an encapsulant led to more severe degradation compared to modules encapsulated with POE on the front and EPE on the rear (~2.1 $\%_{rel}$ for LAF module and ~7.3 $\%_{rel}$ for baseline module) [18]. These results highlight the superior damp-heat durability and performance retention of LAF modules. However, the reliability challenges posed by EVA encapsulants under DH85 testing remain a critical concern.

Fig. 3 presents the EL images of LAF and baseline modules to monitor and identify degradation fingerprints. At the initial state, the EL image of baseline modules exhibits a uniform luminescence pattern across all solar cells, signifying minimal initial defects and consistent electrical properties. The interconnects appear intact, with no significant disruptions in the signal. Similarly, the initial EL image of LAF modules shows uniform luminescence without observable defects or brightness variations, indicating stable and reliable initial electrical performance. After 1000 h of DH85 testing, significant degradation becomes evident in the baseline modules. Several solar cells display extensive dark areas, reflecting a considerable reduction in luminescence and severe electrical performance failures. These dark regions are primarily located near interconnects and busbars, areas typically susceptible to mechanical or environmental stress. Zoomed-in sections of the EL images reveal a high density of localized defects in the metallization, further highlighting critical failure points. This pronounced degradation aligns with vulnerabilities in metallization and interconnects, as observed in previous studies on industrial TOPCon modules by Zhou et al. and Sen et al. [14, 36].

Importantly, the observed degradation was not uniformly distributed across all cells. In mass production, slight variations are inherently introduced during each processing step, and these accumulated differences—amplified through technological superposition—can result in varying sensitivities to damp-heat degradation. For instance, some half-cells located in the bottom and top corners of the modules also showed severe degradation fingerprints. Furthermore, as previously noted, the Al content in the Ag/Al paste ranges from 3 % to 5 %, which may further contribute to inconsistent degradation behavior. These findings suggest that both intrinsic processing variability and positional factors within the module can significantly influence degradation sensitivity under damp-heat stress.

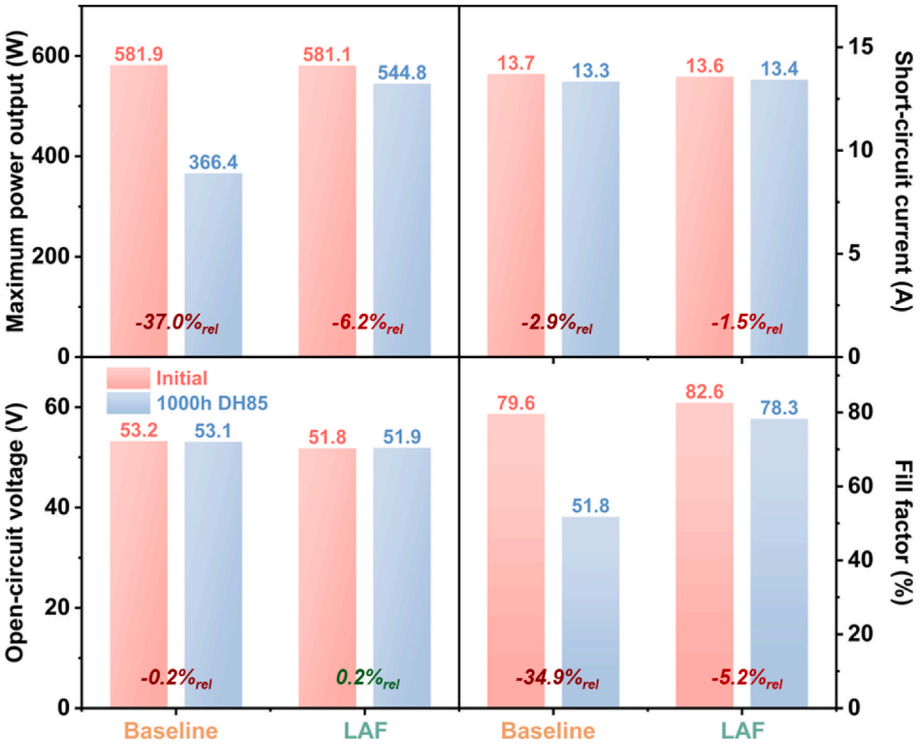

Fig. 2. Electrical parameter degradation of baseline and LAF G-B modules compared to initial measurements after 1000 h of DH85 testing.

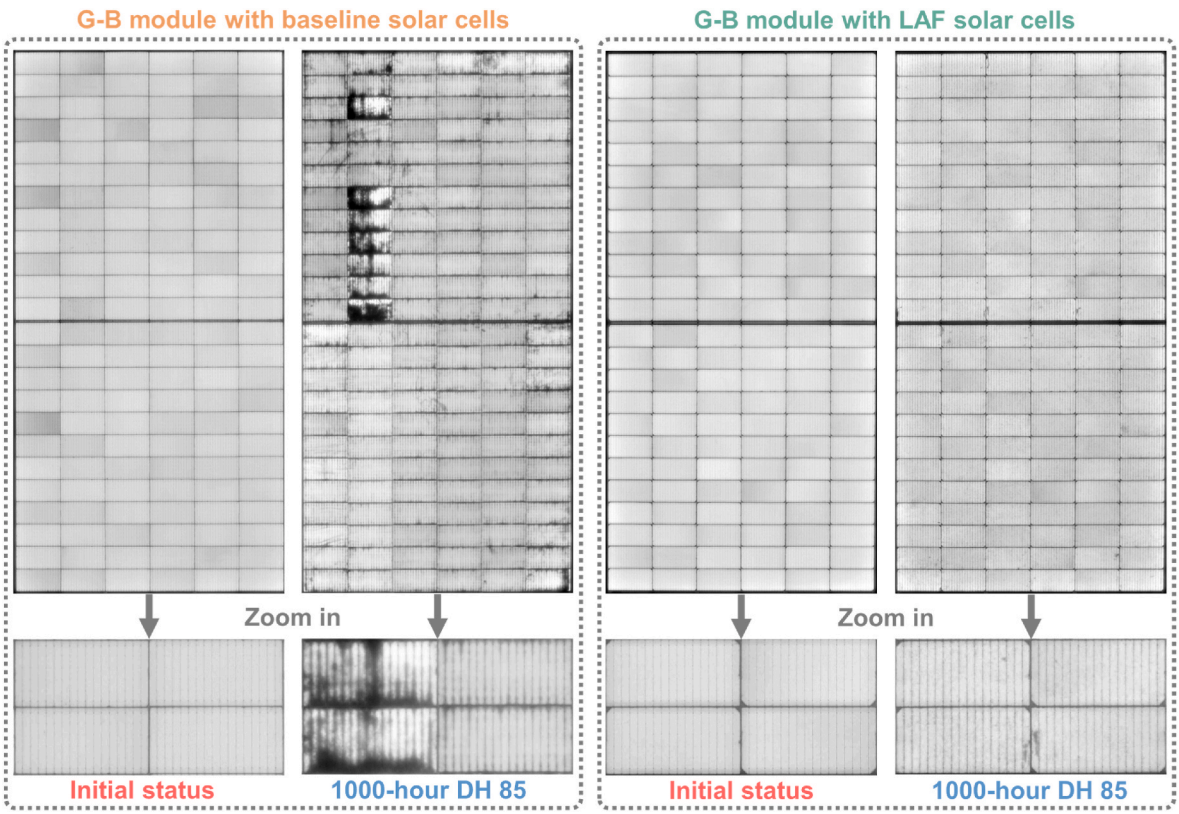

Fig. 3. Electroluminescence images of baseline and LAF G-B modules captured before and after 1000 h of DH85 testing.

In contrast, the LAF modules exhibit a lower degree of degradation after 1000-h DH85 testing. The luminescence intensity across the cells remains largely uniform, with only minor reductions in brightness in localized areas. Some degradation patterns are observed along the metallization, but the absence of widespread dark regions suggests enhanced resistance to environmental stressors. The zoomed-in sections reveal fewer metallization defects, pointing to robust interconnect stability and superior resistance to moisture-induced degradation. The advanced LAF technique demonstrates improved durability under damp-heat stress, likely due to the use of customized Ag paste (with low Al content) and the LAF process. These innovations contribute to stronger contact adhesion and reduced susceptibility to moisture ingress or corrosive reactions, ensuring better long-term performance.

3.2. *FIB-SEM cross-section images*

To further investigate metallization failures, FIB-SEM images were captured from the module samples and compared with control cell samples. Considering the localized nature of FIB-SEM, multiple regions from each group were analyzed, and eight representative images were selected and shown in Fig. 4. This figure provides an overview of the finger structures for each group. For the baseline (BL) control, SEM and EDS analyses clearly identified the presence of Ag and Al particles in the Control-front group, as illustrated in Fig. 4. Notably, Al was primarily observed as clusters embedded within the Ag matrix, aligning with findings from previous studies [27,37,38]. Within the front contact, several prominent Al particles were evident. In industrial TOPCon solar cells, the widespread use of Al/Ag paste for front-side metallization is primarily intended to reduce the contact resistivity between the metal and the boron-doped emitter [27,37,38]. In contrast, LAF solar cells utilized a paste with a reduced Al content (<0.2 at.%), where Al played a minimal role in the formation of ohmic contacts. For both baseline and LAF solar cells, the majority of the glass frit in the front-side contact consisted of lead oxide (PbO), which facilitates the dissolution of silicon nitride layers, enhances mechanical adhesion, optimizes electrical conductivity, and performs other critical functions.

Unlike the front-side paste, no significant Al content was detected in the rear-side pastes. However, tellurium (Te) was present, primarily due to the inclusion of tellurium oxide (TeO_2) in the rear-side paste. TeO_2 functions as a fluxing agent in the metallization paste, lowering the melting temperature of the glass frit and improving adhesion during sintering. It also enhances wetting on the silicon surface, ensuring uniform Ag re-crystallization and better metal-silicon contact. Additionally, TeO_2 reduces contact resistance, improves electrical conductivity, and protects passivation layers, particularly the tunnel oxide, from damage during sintering by forming Ag-Te alloy [39–41]. In this study, TeO_2 was incorporated into the Ag paste to optimize the adaptation to the TOPCon structure and the rear-side etched surface morphology.

The module-level DH85-tested samples showed distinct degradation fingerprints compared to the control samples. Shown in Fig. 4, elemental analysis revealed a noticeable reduction in the Al-to-Ag or Pb-to-Ag ratios on the front side and the Te-to-Ag or Pb-to-Ag ratios on the rear side. To further investigate the degradation mechanisms, high magnification images were taken and shown in Figs. 5 and 6.

Fig. 5 and Supplementary Fig. S1 illustrate cross-sectional SEM images and corresponding EDS elemental mappings of the silicon-metal interface and metal bulk for the front contacts of different experimental groups: BL control-front, BL module DH-front, LAF control-front, and LAF module DH-front. At the silicon-metal interface, the BL control-front sample shows a dense and intact interface, free from any visible defects or corrosion, reflecting the pristine condition of the contact. In contrast, the BL module DH-front sample, subjected to module-level DH85 testing, exhibits distinct regions of corrosion. These corroded regions, highlighted with dashed orange ovals, correspond to areas of accumulated Al and Pb from Supplementary Fig. S1, indicating significant structural degradation likely caused by environmental stress during aging. In the metal bulk, substantial traces of chemical reactions involving Al and Pb are observed, with Al showing extensive oxidation.

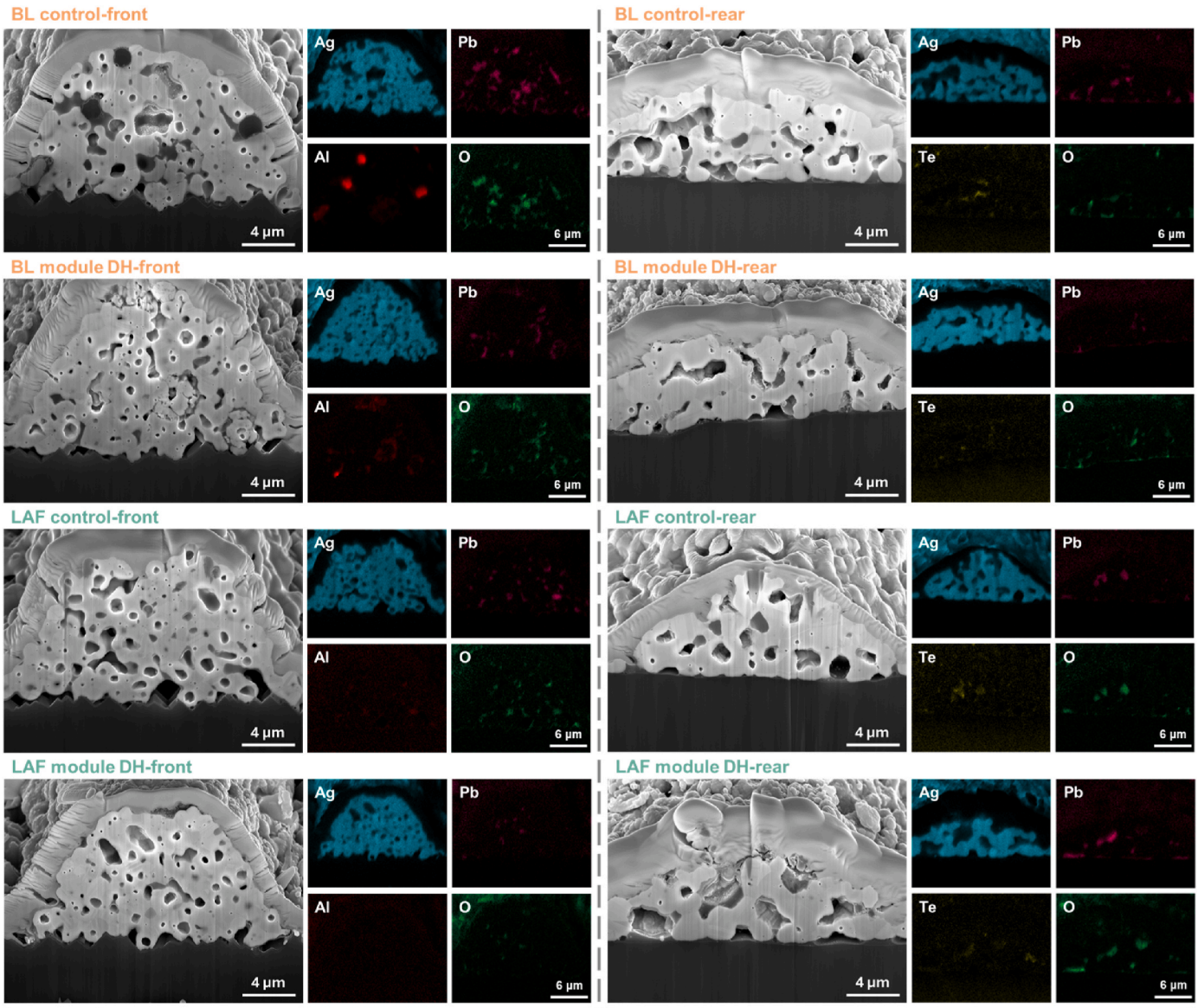

Analyzed element	Front-side atomic ration by EDS analysis			
	BL control	BL module DH	JSIM control	JSIM module DH
C	38.72	38.08	39.85	42.23
N	2.78	4.15	3.3	2.6
O	4.19	4.49	2.9	4.49
Al	1.15	0.2	0.1	0.06
Si	29.85	29.88	30.24	27.83
Ga	1.3	0.88	1.34	1.16
Ag	17.59	18.78	18.1	17.79
Te	0	0	0	0
Pt	4.15	3.4	4	3.76
Pb	0.26	0.12	0.18	0.09
Total	100	100	100	100
Al to Ag ratio ($\times 10^{-2}$)	**6.5**	**1.1**	**0.55**	**0.34**
Pb to Ag ratio ($\times 10^{-2}$)	**1.5**	**0.64**	**0.99**	**0.51**

Analyzed element	Rear-side atomic ration by EDS analysis			
	BL control	BL module DH	JSIM control	JSIM module DH
C	44.76	47.56	40.17	45.45
N	0	1.17	0	0
O	2.08	1.85	2.73	1.32
Al	0	0	0.01	0
Si	33.34	34.17	39.26	35.07
Ga	1.32	0.87	1.14	0.65
Ag	14.2	10.75	13.04	13.83
Te	0.04	0.01	0.03	0.02
Pt	4.13	3.55	3.51	3.61
Pb	0.12	0.07	0.11	0.05
Total	100	100	100	100
Te to Ag ratio ($\times 10^{-2}$)	**0.28**	**0.09**	**0.23**	**0.14**
Pb to Ag ratio ($\times 10^{-2}$)	**0.85**	**0.65**	**0.84**	**0.36**

Fig. 4. 5000 × cross-sectional SEM images with corresponding EDS analysis of the metal contacts from baseline and LAF solar cells, along with module-level degraded samples.

This behaviour is markedly different from the metal bulk of the BL control-front sample, where no such reactions are evident. These findings suggest that the contact degradation in the BL module DH-front sample is primarily driven by a synergistic effect of Al oxidation and glass frit corrosion, which significantly compromises the integrity of the front contact under DH85 conditions.

Similarly, the LAF control-front sample exhibits a stable and undamaged interface. However, the LAF module DH-front sample displays

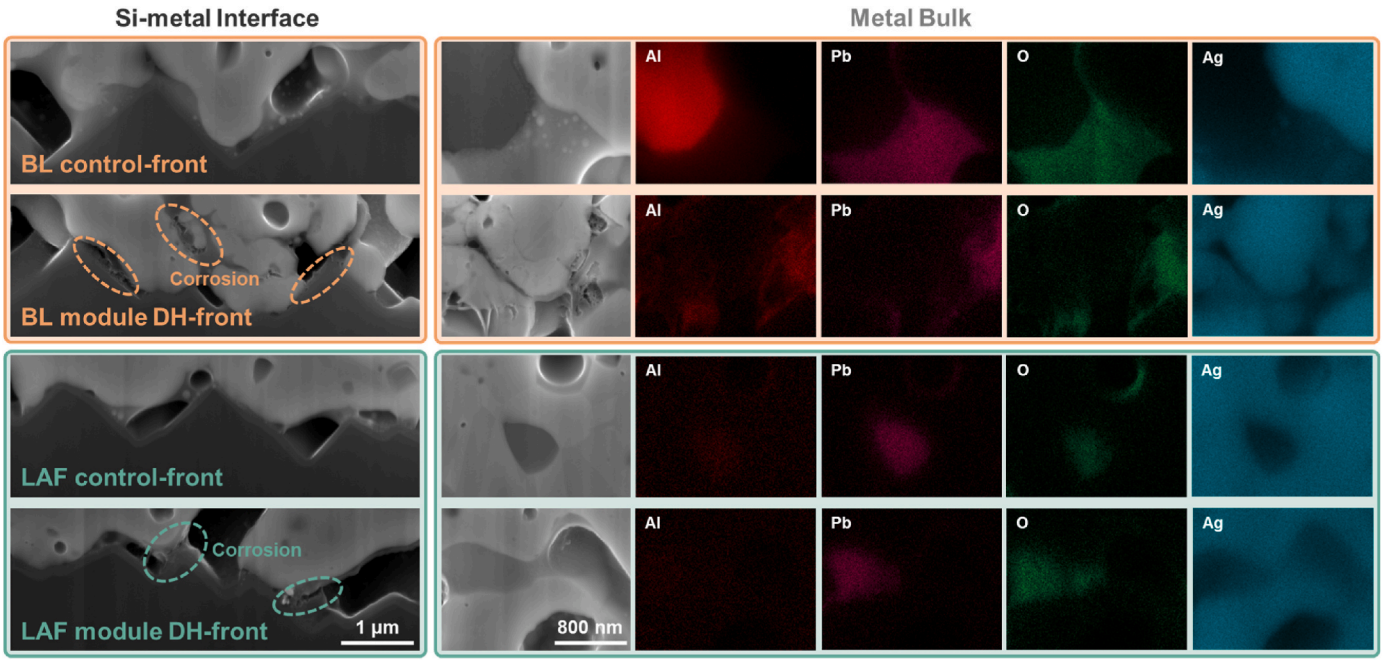

Fig. 5. Cross-sectional SEM images of the metal-Si interfaces in the experimental front contacts at 20,000 × magnification, complemented by 50,000 × magnification images with corresponding EDS analysis of the metal bulk.

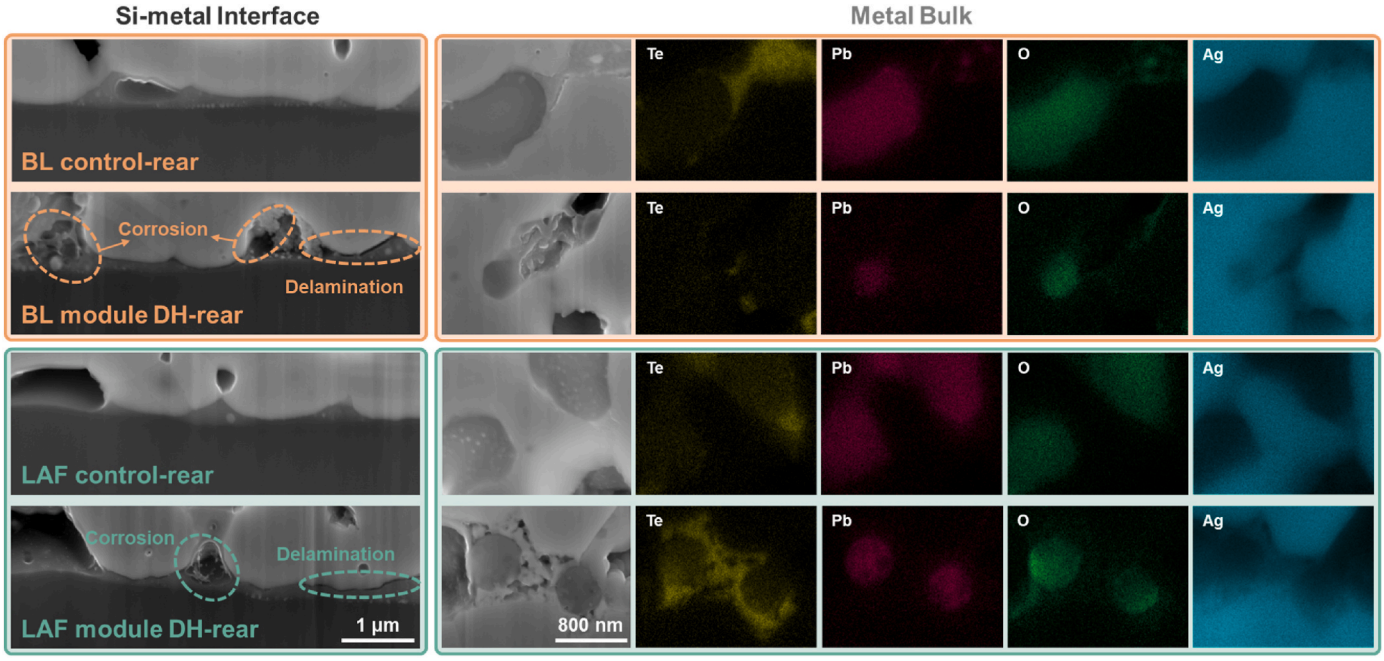

Fig. 6. Cross-sectional SEM images of the metal-Si interfaces in the experimental rear contacts at 20,000 × magnification, complemented by 50,000 × magnification images with corresponding EDS analysis of the metal bulk.

localized corrosion, marked by dashed green ovals, although the extent of degradation is notably less severe than that observed in the BL module DH-front sample. Within the metal bulk of the LAF module DH-front sample, PbO shows no significant shape changes or chemical reaction fingerprints, indicating greater stability compared to the BL module DH-front sample. This improved stability may be attributed to the lower Al content at the interface and within the bulk, resulting in more robust chemical properties under DH85 testing conditions.

Additionally, the rear-side contact analysis is presented in Fig. 6 and Supplementary Fig. S2. For the rear-side application, both BL and LAF solar cells utilized the same industrial Ag paste tailored for the TOPCon rear side. In the rear-side metal paste, the characteristics of Te-containing glasses during fast firing play a critical role in mediating the interactions between Ag and the glass frits. During the firing process, Te within the glass is reduced, leading to the formation of Ag-Te alloys within the molten glass [41,42]. During the formation of the rear-side contact, TeO_2 likely undergoes a reduction reaction, converting to TeO_x (where $x \leq 2$) and forming tellurium-lead-metal-oxygen compounds under high-temperature processing conditions [40,43]. As a result, within the metal bulk, reduced oxygen content is observed in

regions overlapping with Te, aligning with the observations reported by Kim et al. [41]. Additionally, Te is highly concentrated at the interface between PbO and Ag, attributed to its non-metallic properties [40,41,43,44]. Consequently, the BL control-rear and LAF control-rear samples exhibit a dense and intact silicon-metal interface with clear elemental distributions of Ag, Te, and Pb. This indicates strong adhesion of the metal contact to the silicon substrate, with no observable defects or degradation, highlighting the pristine condition of the contact.

In contrast, the BL module DH-rear and LAF module DH-rear samples show significant structural damage, including extensive corrosion and delamination, as highlighted by the dashed ovals. Furthermore, in the metal bulk, Te-rich regions no longer appear dense and intact, whereas the PbO clusters remain stable and unaltered. This suggests that the degradation of rear-side metallization is primarily associated with the instability of Ag-Te alloys.

3.3. Degradation mechanism analysis

Based on previous studies and literature, EVA is highly prone to hydrolysis under damp-heat conditions, leading to the formation of ethylene vinyl alcohol (EVOH) and acetic acid, as illustrated in Fig. 7 (a) [45–48]. The generated acetic acid can cause significant issues, including corrosion of metal contacts, degradation of passivation layers, and even backsheet failure [31,33]. To gain deeper insight into the degradation mechanisms in EVA-encapsulated modules, we subjected baseline and LAF solar cells to an acetic acid mist chamber to evaluate the specific impact of acetic acid on bare solar cells. A comparison of the effects observed in module-level samples and those exposed to acetic acid mist is presented in Fig. 7 (b). Furthermore, EDS analysis of acid mist test samples is shown in Supplementary Fig. S3.

For the front contacts of LAF solar cells, clear evidence of glass-frit decomposition and delamination was observed. Despite the absence of Al content, the glass-frit at the Si-metal interface was highly reactive and prone to corrosion. The potential chemical reaction involved is detailed in Eq. (1), where acetic acid reacts with lead oxide, dissolving the lead oxide and forming lead acetate [33,47]. This dissolution process occurs because acetic acid acts as a weak chelating agent for lead ions. The formation of lead acetate has significant implications, including the dissolution or migration of lead, which can compromise the structural and electrical integrity of solar cells. Furthermore, this reaction alters the interface between the metal contacts and the Si substrate, potentially increasing contact resistance and leading to performance degradation.

$$CH_3COOH_{(aq)} + PbO_{(s)} \rightarrow Pb(CH_3COO)_{2\ (aq)} + H_2O_{(l)} \quad \text{(Eq.1)}$$

Furthermore, the rear-side metallization of the samples subjected to module-level testing shows striking similarities to those exposed to the acid mist test. EDS analysis, when compared to the control samples, revealed structural changes in the Te signal regions, indicating potential corrosion of TeO_x. The chemical mechanism of the reaction between TeO_x and CH_3COOH has not yet been fully understood [49]. According to Iqbal et al., Te compounds are susceptible to reacting with CH_3COOH in moist conditions, leading to the formation of Te salts or compounds with Ag [33]. This reaction causes significant corrosion of the active Te compounds in the glass frit, which impairs its adhesion. Conversely, the higher reactivity of TeO_x in the rear-side metallization results in reduced corrosion of PbO during CH_3COOH exposure. This results in substantial delamination at the metal/Si interface, compromising the integrity of the electrical contacts.

Based on module I-V testing results, failures in both the front and rear metal contacts likely contribute to the decrease in FF. Our previous research shows that Ag/Al in TOPCon solar cells becomes less stable under damp-heat conditions [17,18]. Since Al is more chemically active than Ag and readily loses electrons, a redox reaction occurs between Ag and Al. Additionally, Al is more reactive than Pb, allowing it to undergo a displacement reaction with PbO in the presence of certain ions and moisture. A detailed analysis of these degradation fingerprints and mechanisms was provided in our previous work [17]. The Al accelerates contact corrosion through oxidation and reduction at the front contacts. We also observed that low Al-content Ag paste leads to interface degradation, likely caused by CH_3COOH corrosion of the interface oxides, though at a slower degradation rate compared to Ag/Al paste. For practical applications, incorporating a small amount of Al provides several advantages. First, Al is more cost-effective than Ag, so using a low Al concentration helps to reduce the overall cost of metallization pastes. Second, Al plays a crucial role in the firing process of solar cell fabrication by enabling the paste to penetrate the aluminium oxide (AlO_x) layer, a challenge that pure Ag paste struggles to overcome. This ability enhances contact formation, ensures a more reliable electrical interface, and ultimately improves the manufacturability and stability of solar cells. On the rear side, TeO_x is particularly vulnerable to CH_3COOH-rich damp-heat conditions. Since TeO_x plays a key role in contact formation, its corrosion and corresponding interface delamination can lead to contact failures and a decrease in FF. Therefore, G-B TOPCon modules with EVA encapsulant are highly at risk of degradation under damp-heat conditions. Based on our results, double-sided EVA is currently not a suitable encapsulant for glass-backsheet TOPCon modules exposed to damp-heat conditions, even when combined with LAF-processed cells. Although the use of LAF and low-Al-content paste provides partial mitigation, the degradation observed under DH85

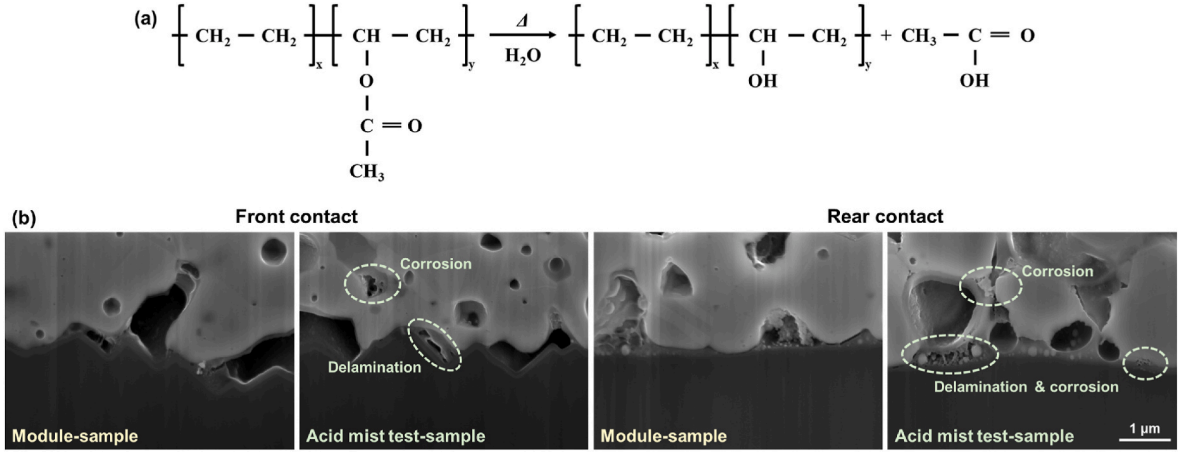

Fig. 7. (a) Schematic representation of EVA polymer hydrolysis under damp-heat conditions, and (b) comparison of metal-silicon interface contacts between samples from module-level testing and acetic acid mist exposure. (For interpretation of the references to colour in this figure legend, the reader is referred to the Web version of this article.)

testing highlights the need for further improvements in both materials and processing. In particular, advancements in front- and rear-side metallization are essential before EVA-based glass-backsheet configurations can be considered viable for widespread deployment in TOPCon technologies.

4. Conclusion

This study investigates the damp-heat degradation of EVA-encapsulated industrial TOPCon solar modules after 1000 h of DH85 exposure. Significant degradation was observed in baseline modules made with Ag/Al paste solar cells, which experienced a ~37.0 % relative power output loss, primarily due to a ~34.9 % reduction in FF. In contrast, LAF modules, which were made with low Al-content Ag paste TOPCon solar cells, showed much smaller degradation (~6.2 $\%_{rel}$) with a lesser reduction in FF. These findings underscore the severe instability of Ag/Al paste, while also revealing that the EVA encapsulant contributes to degradation in low Al-Ag paste TOPCon modules, albeit to a lesser extent.

To further explore the degradation mechanisms, FIB-SEM and corresponding EDS analyses were conducted to examine changes in the metal contacts. In the case of Ag/Al paste contacts, damp-heat conditions, combined with CH_3COOH potentially generated from the EVA, induced significant redox reactions, likely leading to the failure of effective contact. Similarly, low Al-content Ag paste also showed failures, particularly at the glass-front interface. This suggests that EVA-encapsulated environments under damp-heat conditions can lead to the corrosion of the interface glass-frit, resulting in localized ineffective contacts. However, the chemical stability of low Al-content Ag paste is higher than that of Ag/Al paste, resulting in a slower degradation rate for these modules.

Additionally, rear-side contacts were found to be vulnerable under damp-heat conditions. This is primarily due to the reactivity of Te compounds in the glass frit of the rear-side paste. As TeO_x or Te/Ag alloys corrode, rear-side metallization becomes more prone to delamination from the solar cells, which can increase contact resistance.

In summary, the findings indicate that while low Al-content Ag paste modules exhibit less degradation than Ag/Al paste modules under damp-heat conditions, both types of contacts are affected by the EVA encapsulant. Furthermore, rear-side contacts show additional vulnerabilities due to the reactive nature of Te compounds in the glass frit. Nonetheless, by optimizing material formulations and processing methods, further advancements in both performance and cost-effectiveness are anticipated. Future research should focus on refining these strategies, exploring alternative materials, and investigating other environmental stressors to enhance the stability and cost-effectiveness of TOPCon modules, ultimately contributing to the goal of sustainable and affordable solar energy generation.

CRediT authorship contribution statement

Xinyuan Wu: Writing – review & editing, Writing – original draft, Visualization, Validation, Software, Methodology, Investigation, Formal analysis. **Wei Wu:** Resources, Investigation, Formal analysis, Data curation. **Yan Zhang:** Investigation, Formal analysis, Data curation. **Jiexi Fu:** Investigation, Formal analysis. **Xutao Wang:** Methodology, Investigation, Formal analysis. **Jieyi Li:** Visualization, Investigation. **Weiguang Yang:** Methodology, Investigation, Formal analysis. **Feng Li:** Methodology, Investigation. **Lin Lv:** Project administration, Methodology, Investigation. **Jessica Yajie Jiang:** Writing – review & editing, Investigation, Formal analysis. **Bram Hoex:** Writing – review & editing, Supervision, Project administration, Methodology, Investigation, Funding acquisition, Formal analysis, Conceptualization.

Declaration of competing interest

The authors declare the following financial interests/personal relationships which may be considered as potential competing interests: Bram Hoex reports was provided by Australian Centre for Advanced Photovoltaics. If there are other authors, they declare that they have no known competing financial interests or personal relationships that could have appeared to influence the work reported in this paper.

Acknowledgements

This work is supported by the Australian Centre for Advanced Photovoltaics (ACAP) and received funding from the Australian Renewable Energy Agency (ARENA) as well as the Australian Government's Trailblazer for Recycling & Clean Energy program, led by UNSW & the University of Newcastle. However, the Australian Government does not accept responsibility for the views, information, or advice expressed in this research. The authors would like to acknowledge the Electron Microscope Unit at The University of New South Wales (UNSW), specifically Dr Charlie Kong and Dr Yin Yao, for their scientific and technical assistance and access to the facilities of the Australian Microscopy & Microanalysis Research Facility. The authors acknowledge the surface analysis laboratory, Solid State & Elemental Analysis Unit (SSEAU), Mark Wainwright Analytical Centre (MWAC), and UNSW for the support of XPS analysis. The authors also express their gratitude for the support provided by the entire team at the Solar Industrial Research Facility (SIRF) at UNSW. During the preparation of this work, the authors used GPT-4o in order to improve the readability and language of the work. After using this tool, the authors reviewed and edited the content as needed and take full responsibility for the content of the publication.

Appendix A. Supplementary data

Supplementary data to this article can be found online at https://doi.org/10.1016/j.solmat.2025.113650.

Data availability

Data will be made available on request.

References

[1] M. Fischer, M. Woodhouse, P. Baliozian, International Technology Roadmap for Photovoltaic (ITRPV) 2023 Results, VDMA, 2024.
[2] S. Ma, et al., Bi-layer in-situ phosphorus doped poly-Si films by PECVD for blistering-free high-efficiency industrial TOPCon solar cells, Sol. Energy Mater. Sol. Cell. 269 (2024/06/01/2024) 112771, https://doi.org/10.1016/j.solmat.2024.112771.
[3] Y. Fan, et al., Investigation of the Ag–Si contact characteristics of boron emitters for n-tunnel oxide-passivated contact solar cells metallized by laser-assisted current injection treatment, Sol. RRL (2024/06/05 2024) 2400268, https://doi.org/10.1002/solr.202400268 vol. n/a, no. n/a.
[4] B. Liao, et al., Tube-type plasma-enhanced atomic layer deposition of aluminum oxide: enabling record lab performance for the industry with demonstrated cell efficiencies >24, Prog. Photovoltaics Res. Appl. 31 (1) (2023-01-01 2023) 52–61, https://doi.org/10.1002/pip.3607.
[5] B. Liao, et al., Atomic scale controlled tunnel oxide enabled by a novel industrial tube-based PEALD technology with demonstrated commercial TOPCon cell efficiencies > 24%,, Prog. Photovoltaics Res. Appl. 31 (3) (2023-03-01 2023) 220–229, https://doi.org/10.1002/pip.3627.
[6] B. Liao, J. Ge, X. Wu, Q. Wang, R.J. Yeo, Z. Du, Unlocking the potential of boronsilicate glass passivation for industrial tunnel oxide passivated contact solar cells, Prog. Photovoltaics Res. Appl. 30 (3) (2022) 310–317.
[7] Y. Huang, et al., Ultrathin silicon oxide prepared by in-line plasma-assisted N2O oxidation (PANO) and the application for n-type polysilicon passivated contact, Sol. Energy Mater. Sol. Cell. 208 (2020-05-01 2020) 110389, https://doi.org/10.1016/j.solmat.2019.110389.
[8] J. Zheng, et al., Blistering-free polycrystalline silicon carbide films for double-sided passivating contact solar cells, Sol. Energy Mater. Sol. Cell. 238 (2022) 111586.
[9] T. Gao, et al., An industrially viable TOPCon structure with both ultra-thin SiOx and n+-poly-Si processed by PECVD for p-type c-Si solar cells, Sol. Energy Mater. Sol. Cell. 200 (2019-09-01 2019) 109926, https://doi.org/10.1016/j.solmat.2019.109926.

[10] A. Richter, et al., Design rules for high-efficiency both-sides-contacted silicon solar cells with balanced charge carrier transport and recombination losses, Nat. Energy 6 (4) (2021-04-01 2021) 429–438, https://doi.org/10.1038/s41560-021-00805-w.
[11] A. Richter, et al., Tunnel oxide passivating electron contacts as full-area rear emitter of high-efficiency p-type silicon solar cells, Prog. Photovoltaics Res. Appl. 26 (8) (2018) 579–586.
[12] S. Ma, et al., Improving the performance of industrial TOPCon solar cells through the insertion of intrinsic a-Si layer, Sol. Energy Mater. Sol. Cell. 275 (2024) 113024.
[13] Trinasolar Announces Efficiency of 26.58% for n-type TOPCon Cells, Setting the 28th World Record. https://static.trinasolar.com/us/resources/newsroom/Trinasolar-Sets-28th-World-Record.
[14] C. Sen, et al., Buyer aware: three new failure modes in TOPCon modules absent from PERC technology, Sol. Energy Mater. Sol. Cell. 272 (2024) 112877.
[15] Y. Zhou, D. Chen, Y. Ye, H. Yin, X. Niu, Damp-heat endurance investigation of PV modules based on n-type bifacial passivated contact cells, in: European Photovoltaic Solar Energy Conference and Exhibition 2023, 2023, https://doi.org/10.4229/EUPVSEC2023/3AV.2.41.
[16] Y. Ye et al., "Damp-Heat Stability Investigation of Glass-Backsheet Modules Based on Topcon Solar Cells," *Available at: SSRN 4986461*.
[17] X. Wu, et al., Unveiling the origin of metal contact failures in TOPCon solar cells through accelerated damp-heat testing, Sol. Energy Mater. Sol. Cell. 278 (2024/12/01/2024) 113188, https://doi.org/10.1016/j.solmat.2024.113188.
[18] X. Wu, et al., Enhancing the reliability of TOPCon technology by laser-enhanced contact firing, Sol. Energy Mater. Sol. Cell. 271 (2024/07/01/2024) 112846, https://doi.org/10.1016/j.solmat.2024.112846.
[19] T. Fellmeth, et al., Laser-enhanced contact optimization on iTOPCon solar cells, Prog. Photovoltaics Res. Appl. 30 (12) (2022) 1393–1399.
[20] Q. Wang, K. Guo, S. Gu, W. Huang, W. Wu, J. Ding, Investigation on Effects of the Laser-Enhanced Contact Optimization Process With Ag Paste in a Boron Emitter for n-TOPCon Solar Cell, Progress in Photovoltaics: Research and Applications 33 (2) (2025) 294–308.
[21] S. Großer, E. Krassowski, S. Swatek, H. Zhao, C. Hagendorf, Microscale contact formation by laser enhanced contact optimization, IEEE J. Photovoltaics 12 (1) (2021) 26–30.
[22] E. Krassowski, S. Großer, M. Turek, A. Henning, H. Zhao, Investigation of monocrystalline p-type PERC cells featuring the laser enhanced contact optimization process and new LECO paste, AIP Conf. Proc. 2367 (1) (2021). AIP Publishing.
[23] E. Krassowski, T. Luka, V. Naumann, M. Turek, S. Großer, H. Zhao, Degradation stability of solar cells after laser enhanced contact optimization (LECO), AIP Conf. Proc. 2487 (1) (2022). AIP Publishing.
[24] A. Mette, et al., Q.ANTUM NEO with LECO exceeding 25.5 % cell efficiency, Sol. Energy Mater. Sol. Cell. 277 (2024/10/15/2024) 113110, https://doi.org/10.1016/j.solmat.2024.113110.
[25] G. Xing, W. Chen, Y. Liu, X. Du, Al-induced variation to Ag crystal orientation of Ag–Al pastes during metallization, Sol. Energy Mater. Sol. Cell. 270 (2024/06/15/2024) 112814, https://doi.org/10.1016/j.solmat.2024.112814.
[26] N. Wöhrle, E. Lohmüller, J. Greulich, S. Werner, S. Mack, Towards understanding the characteristics of Ag–Al spiking on boron-doped silicon for solar cells, Sol. Energy Mater. Sol. Cell. 146 (2016) 72–79.
[27] F. Kiefer, J. Krügener, F. Heinemeyer, H.J. Osten, R. Brendel, R. Peibst, Structural investigation of printed Ag/Al contacts on silicon and numerical modeling of their contact recombination, IEEE J. Photovoltaics 6 (5) (2016) 1175–1182.
[28] S. Uličná, A. Sinha, D.C. Miller, B.M. Habersberger, L.T. Schelhas, M. Owen-Bellini, PV encapsulant formulations and stress test conditions influence dominant degradation mechanisms, Sol. Energy Mater. Sol. Cell. 255 (2023/06/15/2023) 112319, https://doi.org/10.1016/j.solmat.2023.112319.
[29] P.M. Sommeling, J. Liu, J.M. Kroon, Corrosion effects in bifacial crystalline silicon PV modules; interactions between metallization and encapsulation, Sol. Energy Mater. Sol. Cell. 256 (2023/07/01/2023) 112321, https://doi.org/10.1016/j.solmat.2023.112321.
[30] O.K. Segbefia, A.G. Imenes, T.O. Sætre, Moisture ingress in photovoltaic modules: a review, Sol. Energy 224 (2021/08/01/2021) 889–906, https://doi.org/10.1016/j.solener.2021.06.055.
[31] M.C.C. de Oliveira, A.S.A.D. Cardoso, M.M. Viana, V.d.F.C. Lins, The causes and effects of degradation of encapsulant ethylene vinyl acetate copolymer (EVA) in crystalline silicon photovoltaic modules: a review, Renew. Sustain. Energy Rev. 81 (2018) 2299–2317.
[32] L. Spinella, et al., Chemical and mechanical interfacial degradation in bifacial glass/glass and glass/transparent backsheet photovoltaic modules, Prog. Photovoltaics Res. Appl. 30 (12) (2022) 1423–1432.
[33] N. Iqbal, et al., Impact of acetic acid exposure on metal contact degradation of different crystalline silicon solar cell technologies, Sol. Energy Mater. Sol. Cell. 250 (2023/01/15/2023) 112089, https://doi.org/10.1016/j.solmat.2022.112089.
[34] IEC TS 62782, 2016 Photovoltaic (PV) Modules - Cyclic (Dynamic) Mechanical Load Testing, I. E. Commission, 2016-03-09 2016 [Online]. Available: https://webstore.iec.ch/publication/24310.
[35] S. Burgess, P. Pinard, AZtec wave–a new way to achieve combined EDS and WDS capability on SEM, Microsc. Microanal. 26 (S2) (2020) 114–115.
[36] Y. Zhou, D. Chen, Y. Ye, H. Yin, X. Niu, Damp-Heat Endurance Investigation of PV Modules Based on N-type Bifacial Passivated Contact Cells, EU PVSEC, 2023, p. 2023, https://doi.org/10.4229/EUPVSEC2023/3AV.2.41.
[37] S. Fritz, M. König, S. Riegel, A. Herguth, M. Hörteis, G. Hahn, Formation of Ag/Al screen-printing contacts on B emitters, IEEE J. Photovoltaics 5 (1) (2014) 145–151.
[38] L. Liang, Z. Li, L.K. Cheng, N. Takeda, R. Young, A. Carroll, Current conduction mechanism of front-side contact of N-type crystalline Si solar cells with Ag/Al pastes, IEEE J. Photovoltaics 4 (2) (2013) 549–553.
[39] J. Zhou, J. Zhang, B. Lv, Firing behavior of lead-containing and lead-free metallization silver paste for monocrystalline silicon solar cells, Sol. Energy Mater. Sol. Cell. 259 (2023) 112439.
[40] A. Ebong, N. Bezawada, K. Batchu, Understanding the influence of tellurium oxide in front Ag paste for contacting silicon solar cells with homogeneous high sheet resistance emitter, Jpn. J. Appl. Phys. 56 (8S2) (2017).
[41] Y. Kim, T. Nakayama, H. Kim, Effect of Te-based glass on contact formation and electrical properties in Si solar cells, J. Alloys Compd. 829 (2020) 154500, https://doi.org/10.1016/j.jallcom.2020.154500, 2020/07/15/.
[42] J. Zhang, J. Zhou, J. Huang, B. Lv, Effect of TeO2-based lead-free glass on contact formation of front side silver metallization for monocrystalline silicon solar cells, Sol. Energy Mater. Sol. Cell. 238 (2022/05/01/2022) 111585, https://doi.org/10.1016/j.solmat.2022.111585.
[43] K.R. Mikeska, M. Lu, W. Liao, Tellurium-based screen-printable conductor metallizations for crystalline silicon solar cells, Prog. Photovoltaics Res. Appl. 27 (12) (2019) 1071–1080.
[44] A. Ebong, W. Zhang, P. Bokalo, A. Rohatgi, Development of a low temperature silver paste for high efficiency screen-printed solar cells, in: Proceedings of the 21st European Photovoltaic Solar Energy Conference and Exhibition, vol. 4, Dresden, 2006.
[45] A.W. Czanderna, F.J. Pern, Encapsulation of PV modules using ethylene vinyl acetate copolymer as a pottant: a critical review, Sol. Energy Mater. Sol. Cell. 43 (2) (1996/09/01/1996) 101–181, https://doi.org/10.1016/0927-0248(95)00150-6.
[46] F. Pern, A. Czanderna, Characterization of ethylene vinyl acetate (EVA) encapsulant: effects of thermal processing and weathering degradation on its discoloration, Sol. Energy Mater. Sol. Cell. 25 (1–2) (1992) 3–23.
[47] M.D. Kempe, G.J. Jorgensen, K.M. Terwilliger, T.J. McMahon, C.E. Kennedy, T. T. Borek, Acetic acid production and glass transition concerns with ethylene-vinyl acetate used in photovoltaic devices, Solar energy materials and solar cells 91 (4) (2007) 315–329.
[48] M.D. Kempe, Modeling of rates of moisture ingress into photovoltaic modules, Sol. Energy Mater. Sol. Cell. 90 (16) (2006/10/16/2006) 2720–2738, https://doi.org/10.1016/j.solmat.2006.04.002.
[49] W. Dutton, W.C. Cooper, The oxides and oxyacids of tellurium, Chem. Rev. 66 (6) (1966) 657–675.